ACS APPLIED MATERIALS & INTERFACES

Letter

www.acsami.org

# Enhancement of Heating Performance of Carbon Nanotube Sheet with Granular Metal

Hyeongwook Im,[†] Eui Yun Jang,[†] Ajeong Choi,[‡] Wal Jun Kim,[†] Tae June Kang,*[,†] Yung Woo Park,[‡] and Yong Hyup Kim*[,†]

[†]School of Mechanical and Aerospace Engineering and [‡]Department of Physics and Astronomy, Seoul National University, Seoul 151-744, South Korea

**ABSTRACT:** A strategy for enhancing the heating performance of freestanding carbon nanotube (CNT) sheet is presented that involves decorating the sheet with granular-type palladium (Pd) particles. When Pd is added to the sheet, the heating efficiency of CNT sheet is increased by a factor of 3.6 (99.9 °C cm$^2$/W vs 27.3 °C cm$^2$/W with no Pd). Suppression of convective heat transfer loss attributes to the enhanced heat generation efficiency. However, higher heating response of CNT/Pd sheet was observed compared to CNT sheet, hence suggesting that the electron−lattice energy exchange could be additional heating mechanism in the presence of granular-type particles of Pd having a diameter of 10 nm or less. CNT sheet/Pd is quite stable, retaining its initial characteristics even after 300 cycles of on−off voltage pulses and shows fast thermal responses of the heating and cooling rates being 154 and −248 °C/s, respectively.

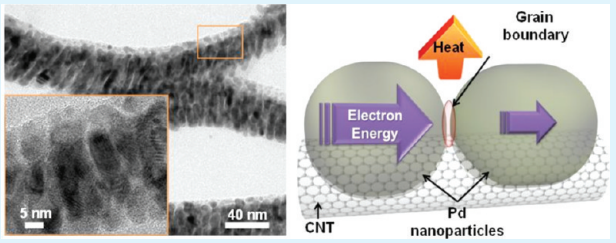


**KEYWORDS:** *carbon nanotube sheet, granular-type palladium, electron−lattice energy exchange*

## 1. INTRODUCTION

Since the first synthesis of carbon nanotube (CNT) forest that can be drawn as a yarn[1] and demonstration that large area CNT aerogel sheets can be drawn from similar forests,[2] forest-drawn CNT sheets have been studied for various applications, including optical polarizers,[1−5] touch screens,[6] microheaters,[7] sound generators,[8,9] and various other devices.[10−14] High intensity, broad spectrum, nonresonant sound generation can be produced using the thermoacoustic effect, in which the ultralow density and high gravimetric surface area of the aerogel sheets optimizes the pressure oscillations induced by electrically produced temperature oscillations.[15] Similarly, when these sheets are used as microheaters, fast thermal response, low power consumption, and excellent stability results are expected.

Inelastic electron scattering at interfaces, known as electron−lattice energy exchange or electron−phonon interaction, is one of the basic processes for electron−phonon interactions in thin film, nanostructured, and low-dimensional conductors. Electron−lattice energy exchange, which causes energy transfer at interfaces, plays an important role in the heat generation in resistive heaters.[16,17] According to previous studies, electron−phonon interactions are strongly increased because of confinement effects for metal clusters[18−20] having a diameter of 10 nm or less.[21]

Many recent investigations have focused on utilizing CNTs with functional guests.[22,23] By effectively combining unique properties of guest materials with superior mechanical, thermal, and electrical characteristics of CNTs, remarkable results in various fields have been obtained.[22−25] Commercial thin film heaters utilize platinum, which motivated us to introduce a metal as a guest material. Palladium (Pd) is less expensive than platinum and not oxidized up to 1070 K.[26] Furthermore, it has excellent thermal and electrical properties.

Decoration of the CNT sheet with Pd could be accomplished by two techniques: reduction−oxidation (redox) reaction and physical vapor deposition (PVD). For redox reaction, it is necessary to generate defect sites on CNT walls through acid pretreatment.[27] Therefore, this method can damage the inherent properties of CNTs. On the other hand, PVD methods like thermal evaporation and sputtering, which physically place a metal layer onto CNT without damage, have the advantage of controlling the deposition volume and particle size. Moreover, this method is especially suitable for mass production.

Recently, various efforts have been made to develop heaters based on carbon nanomaterials, such as CNT[7,28−31] and graphene[32] because of their extraordinary thermal properties. In this paper, we present a strategy for enhancing the heating performance of freestanding CNT sheet by decorating it with palladium. When Pd is added to the CNT sheet, the heating performance is greatly enhanced; yielding a heating efficiency that is higher than tripled. It can be thought that this is only attributed to suppression of convective heat loss into surrounding air. However, increased heating response after Pd decoration suggests that the Pd has a contribution to heat generation. The deposited Pd forms granular arrays along the CNT bundles that comprise the sheet, and functions as electron channels. Electrons that pass through the granular Pd

**Received:** March 17, 2012
**Accepted:** April 25, 2012
**Published:** April 25, 2012

  

channels interact with the lattice of particle interface, resulting in the transformation of electron energy into heat, as schematically illustrated in Figure 1b. As a result, enhanced

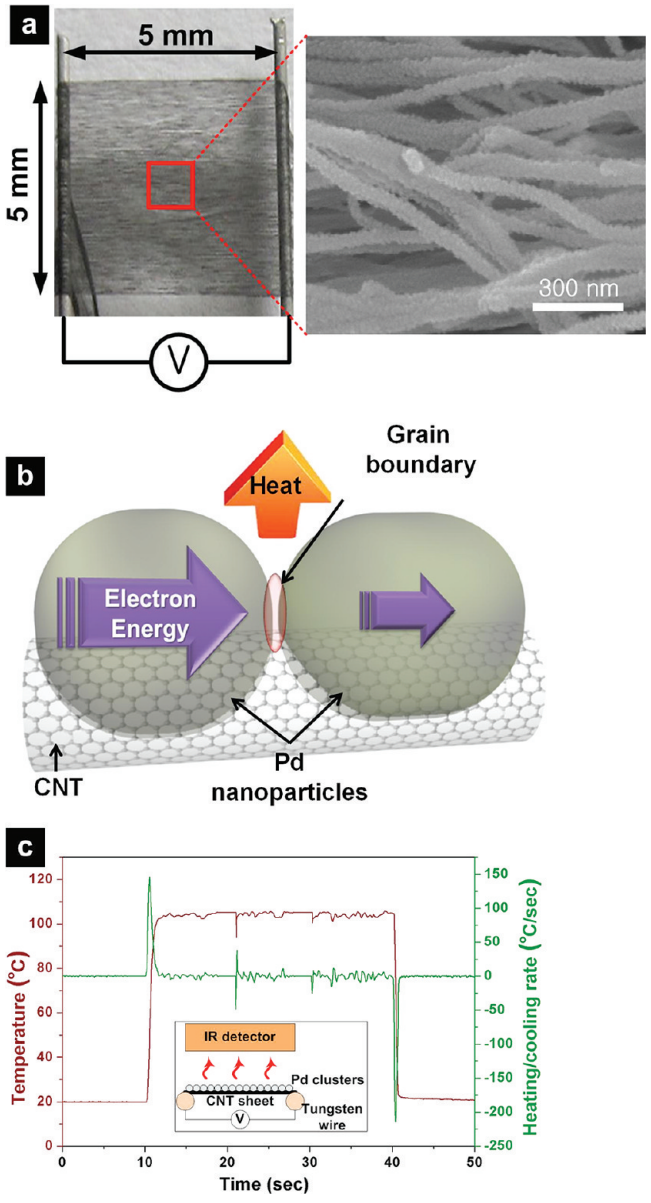


**Figure 1.** (a) Left: optical image of freestanding CNT/Pd sheet. Right: detailed view of CNT/Pd sheet. (b) Schematic of heat generation by electron−lattice energy exchange in Pd nanoparticles on CNT. (c) Temperature profile with time and its derivative (heating/cooling rate) of CNT/Pd sheet with applied voltage of 5.5 V. Inset: experimental setup for temperature measurement.

efficiency is attributed to suppression of convective loss as well as heat generation of Pd nanoparticles. Heating response of CNT sheet is improved by the presence of Pd. After 300 cycles of on−off pulse of voltage, the CNT/Pd sheet is quite stable, retaining its initial characteristics.

## 2. EXPERIMENTAL SECTION

**2.1. Preparation of Freestanding CNT/Pd Sheet.** Vertically aligned multiwalled carbon nanotube (MWCNT) arrays were grown on an iron-catalyst-coated silicon substrate by chemical vapor deposition of acetylene gas. The diameter and height of MWCNTs are ∼10 nm and ∼200 μm, respectively. CNT sheets were drawn from a sidewall of the MWCNT forests using the dry-state spinning process,[2,11] which typically have a density of ∼1.5 mg/cm$^3$, an areal density in the sheet plane of ∼1 to ∼3 mg/cm$^2$. The as-produced CNT sheet was suspended between two tungsten wires. Then, a 100 nm thick layer of Pd metal was deposited by the thermal evaporation method. The freestanding CNT/Pd sheet has a suspended area of 5 mm ×5 mm as shown in Figure 1a.

**2.2. Experimental Setup and Instrumentation.** An infrared (IR) thermal detector (NEC Avio, TVS-500EX), which has a lateral resolution of 0.7 mm at measurement distance of 30 cm, was utilized for in situ measurements of electrically generated temperature profiles. The temperature dependence of the electrical resistivity was investigated in the range between 8 and 300 K under 1.33 × 10$^{-1}$ Pa pressure. Temperature was controlled using a variable temperature cryogenic system (Janis, ST-100).

The surface morphology of the sheet was observed by field-emission scanning electron microscopy (FE-SEM, Hitachi-S4800) and high-resolution transmission electron microscopy (HR-TEM, JEM-3000F). The change in the electrical resistance before and after Pd deposition on CNT sheet was evaluated by *I*−*V* measurement.

## 3. RESULTS AND DISCUSSION

A freestanding CNT/Pd sheet was fabricated by mechanical draw from a CNT forest and then thermal evaporation of a 100 nm thick Pd metal layer on the sheet (see Experimental Section for details). Figure 1a shows an optical image of the freestanding CNT/Pd sheet formed between two tungsten wires. Detailed view of CNT/Pd sheet is depicted in the right of Figure 1a. The temperature profile and heating/cooling rates of the CNT/Pd sheet (applied voltage of 5.5 V) are shown in Figure 1c. The heating/cooling rates can be obtained from the derivative of the temperature profile. For a steady-state temperature of 105 °C, the heating/cooling rates of the CNT/Pd sheet are 154 and −248 °C/s, respectively, as shown in the figure. These fast thermal responses are due to very low thermal capacity[15] and the giant gravimetric surface area of the carbon nanotube sheets. The temperature measurement setup based on an infrared (IR) detector is schematically illustrated in the inset of Figure 1c. The IR thermal detector was located 30 cm above the sample. All experiments were carried out at room temperature under atmospheric conditions. The surface temperature of the sheet was evaluated from the IR radiation emitted from the CNT or Pd cluster, which is based on emissivity of them (0.94, 0.86, respectively). The emissivity of all samples was calibrated using the temperature measured by thermocouples. The steady-state temperature was averaged over the entire sheet area.

Current−voltage (I−V) measurements before and after deposition of Pd on CNT sheet reveal that the electrical resistance of the CNT sheet is greatly reduced from 3.18 kΩ to 0.147 kΩ after deposition of Pd. The reduced electrical resistance coms from reduced contact resistance between CNTs as well as formation of electrical path of granular Pd. Figure 2a, b show scanning electron microscopy (SEM) images of a CNT sheet before and after deposition of Pd, respectively. After Pd deposition, the diameter of CNT bundle increases and the surface becomes rough. It has been reported that Pd films are conformally coated on suspended CNT due to strong binding energy between metal atoms and CNT.[33] It can be


dx.doi.org/10.1021/am300477u | ACS Appl. Mater. Interfaces 2012, 4, 2338−2342

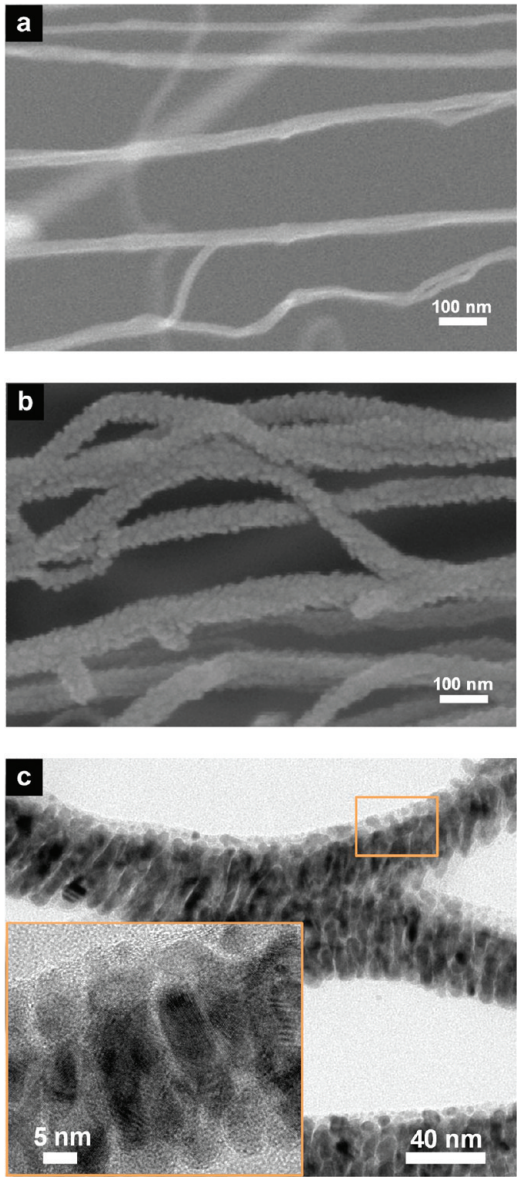


**Figure 2.** SEM images of CNT sheet (a) before and (b) after Pd deposition. (c) TEM image of morphology of deposited Pd on CNT sheet. Inset: magnified view of a rectangular part in the figure. The diameters of deposited Pd nanoparticles are about 10 nm or less.

thought that Pd metal grown on curved surface of CNT bundle forms grain boundaries and finally grows into particles. Transmission electron microscopy (TEM) images of CNT/Pd sheet in Figure 2c shows that densely packed and cluster shape of Pd nanoparticles are deposited on CNT bundles. The diameter of Pd nanoparticles is measured to be 5−10 nm by TEM analysis.

The heating performance of CNT #1, CNT #20 and CNT/Pd sheet is given in Figure 3a, where #1, #20 and CNT/Pd denote 1, 20 layers of CNT sheet, and a Pd-decorated one-layer CNT sheet, respectively. The CNT #20 sheet has a resistance of 145 Ω that is almost the same as that of CNT/Pd sheet (147 Ω). These results clearly reveal a much better heating performance of the CNT/Pd sheet over the CNT #1. In fact, the efficiency of the CNT/Pd sheet is 99.9 °C cm$^2$/W, whereas it is 27.3 °C cm$^2$/W for the CNT #1 sheet, a 3.6 fold increase in efficiency. Moreover, the CNT/Pd sheet shows a better

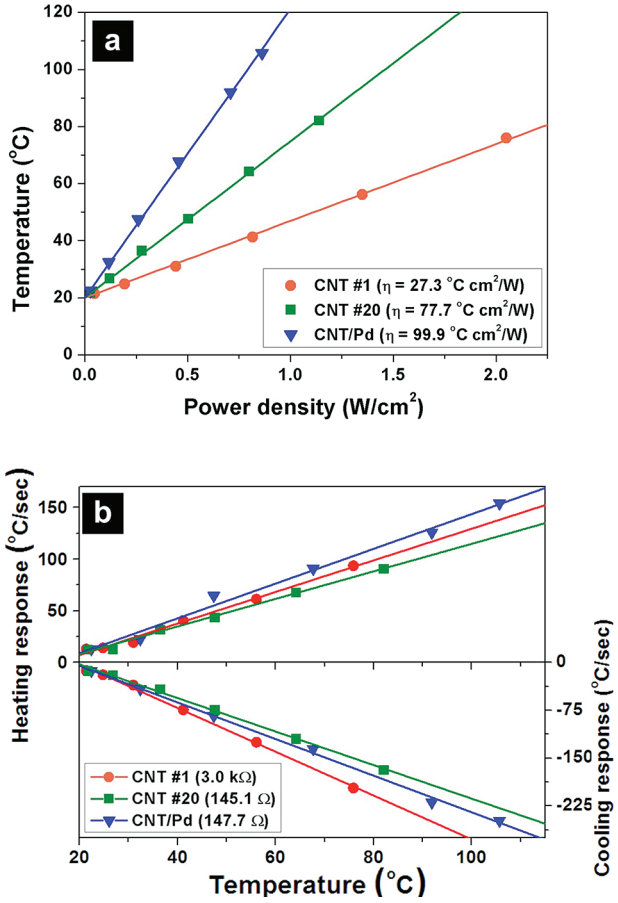


**Figure 3.** (a) Heating performance of the CNT #1, CNT #20, and CNT/Pd sheet. (b) Thermal response with respect to the steady-state temperature of the samples.

efficiency by a factor of 1.3 than CNT #20 sample, although the resistance is practically the same for both.

The heating/cooling responses of the samples as a function of steady-state temperature are presented in Figure 3b. The heating/cooling rates have a linear relationship with temperature. The cooling response curves in the figure can be explained in terms of thermal mass, the mass of CNT #1 being the lowest and that of CNT #20 being the highest. The temperature change induced by electrical input depends on thermal capacitance per area, thus the CNT #1 is expected to provide high thermal response. It is clear that suppression of convective loss attributes to the enhanced heat generation efficiency in 20 layers of CNT sheet. Suppression of the thermal losses also takes place in the CNT/Pd sheet. However, it is observed that the CNT/Pd sheet shows faster heating response compared to that of CNT #1 as shown in Figure 3b, even though the CNT/Pd sheet has larger thermal capacitance. This enhanced heating rate might be explained in terms of electron−phonon interaction raking place in the nanoparticle array of Pd that leads to heating, as explained below.

As shown in Figure 4a, the temperature dependence of resistivity of CNT #1 is quite different from that of the CNT/Pd sheet. The resistivity of CNT #1 sheet decreases with increasing temperature, showing a negative temperature coefficient of resistivity, $d\rho/dT < 0$.[2,34] For the CNT/Pd sheet, however, resistance increases with temperature ($d\rho/dT > 0$), which is in good agreement with previous results[35,36] on metallic granular film and indicates that granular structure acts


dx.doi.org/10.1021/am300477u | ACS Appl. Mater. Interfaces 2012, 4, 2338−2342

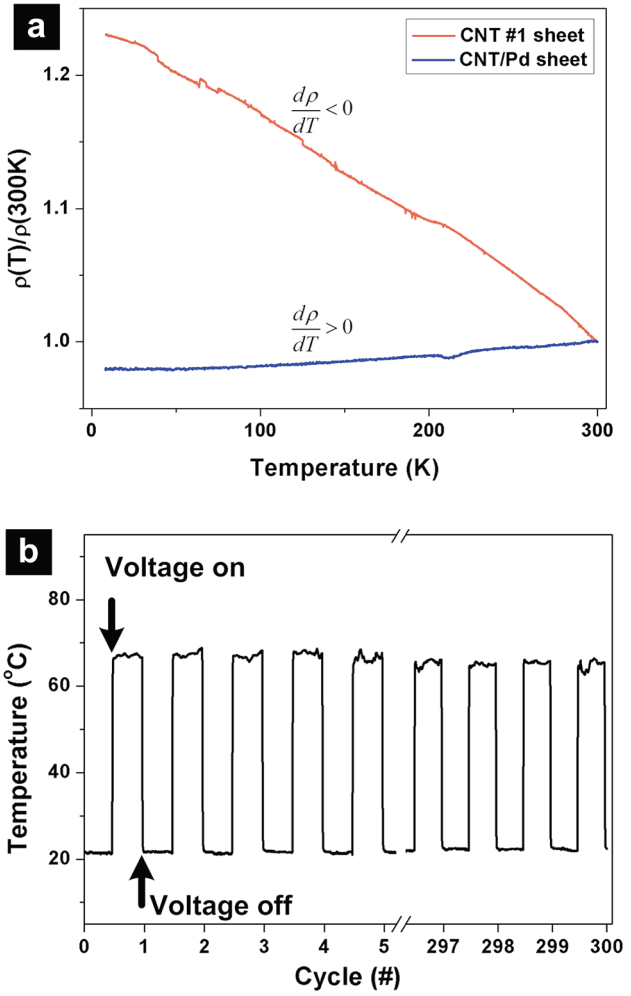


**Figure 4.** (a) Normalized temperature dependence of resistivity of CNT #1 and CNT/Pd sheet. (b) Stability test of CNT/Pd sheet. Pulse voltage of 4 V with an on/off period of 20 s was applied 300 times.

as an electron channel. This inferred that electrons that pass through the channel interact with Pd nanoparticle array. According to the previous report,[19−21] electron−lattice energy exchange for metal nanoparticles smaller than 10 nm strongly increases because of confinement effects.[16,17] Hence, the increased heating rate of the CNT/Pd sheet that results with the addition of Pd clusters could be ascribed to the interaction of electrons with lattice at numerous grain boundaries. Further studies are necessary to better understand the contribution of the Pd nanoparticles.

For practical implementation of the CNT/Pd sheet heaters, the heat transfer as well as heat generation properties should be considered. The thermal conductivity of the CNT sheet was reported as 50 ± 5 W/m·K in the previous report,[34] which is quite lower than that of individual CNT. The thermal conductivity in the sheet is mainly limited by dangling terminals and weak van der Waals contacts between CNTs. The thermal conductivity of Pd is known as ∼72 W/m K. Therefore, heat transfer of CNT sheet might be improved slightly after Pd decoration.

To test the stability, the CNT/Pd was subjected to repeated heating and cooling cycles in which a bias of 4 V is applied for 10 s and then turned off for 10 s. The test result is shown in Figure 4b where the temperature and voltage profiles are given as a function of cycle. It can be seen that the thermal response is stable even after 300 cycles.

## 4. CONCLUSION

We have presented a strategy for enhancing the heating performance of freestanding CNT sheet by depositing on the sheet a thin layer of granular-type metal. When palladium is used, the CNT sheet/Pd delivers an efficiency of 99.9 °C cm$^2$/W, which is more than triple, the efficiency without Pd. The remarkable improvement can be attributed to the electron−lattice interaction and suppression of heat loss of Pd nanoparticles. The CNT/Pd sheet responds fast to applied voltage; the heating and cooling rates are 154 and −248 °C/s, respectively. The sheet is also shown to be stable when subjected 300 on/off voltage pulse cycles.

## AUTHOR INFORMATION

### Corresponding Author

*E-mail: yongkim@snu.ac.kr (Y.H.K.); taejunekang@snu.ac.kr (T.J.K.). Tel.: +82-2-880-7385. Fax: +82-2-880-1728.

### Notes

The authors declare no competing financial interest.

## ACKNOWLEDGMENTS

This research was supported by the National Research Foundation of Korea (Grants 2011-0018905, 2011-0001293, 2011-0000318, and 2011-0024818), Defense Acquisition Program Administration and Agency for Defense Development under Contract UD100048JD, K-water Research & Business Project (K_RBP-1), and a grant from the second stage of the Brain Korea 21 Project in 2011. The authors also acknowledge support from the Institute of Advanced Aerospace Technology at Seoul National University.

## REFERENCES

(1) Jiang, K.; Li, Q.; Fan, S. *Nature* **2002**, *419*, 801−801.
(2) Zhang, M.; Fang, S.; Zakhidov, A. A.; Lee, S. B.; Aliev, A. E.; Williams, C. D.; Atkinson, K. R.; Baughman, R. H. *Science* **2005**, *309*, 1215−1219.
(3) Kyoung, J.; Jang, E. Y.; Lima, M. D.; Park, H. R.; Robles, R. O.; Lepró, X.; Kim, Y. H.; Baughman, R. H.; Kim, D. S. *Nano Lett.* **2011**, *11*, 4227−4231.
(4) Liu, K.; Sun, Y.; Chen, L.; Feng, C.; Feng, X.; Jiang, K.; Zhao, Y.; Fan, S. *Nano Lett.* **2008**, *8*, 700−705.
(5) Kai, L.; Yinghui, S.; Peng, L.; Jiaping, W.; Qunqing, L.; Shoushan, F.; Kaili, J. *Nanotechnology* **2009**, *20*, 335705.
(6) Feng, C.; Liu, K.; Wu, J. S.; Liu, L.; Cheng, J. S.; Zhang, Y.; Sun, Y.; Li, Q.; Fan, S.; Jiang, K. *Adv. Funct. Mater.* **2010**, *20*, 885−891.
(7) Liu, P.; Liu, L.; Jiang, K.; Fan, S. *Small* **2011**, *7*, 732−736.
(8) Xiao, L.; Chen, Z.; Feng, C.; Liu, L.; Bai, Z.-Q.; Wang, Y.; Qian, L.; Zhang, Y.; Li, Q.; Jiang, K.; Fan, S. *Nano Lett.* **2008**, *8*, 4539−4545.
(9) Aliev, A. E.; Lima, M. D.; Fang, S.; Baughman, R. H. *Nano Lett.* **2010**, *10*, 2374−2380.
(10) Zhang, L.; Feng, C.; Chen, Z.; Liu, L.; Jiang, K.; Li, Q.; Fan, S. *Nano Lett.* **2008**, *8*, 2564−2569.
(11) Aliev, A. E.; Oh, J.; Kozlov, M. E.; Kuznetsov, A. A.; Fang, S.; Fonseca, A. F.; Ovalle, R.; Lima, M. D.; Haque, M. H.; Gartstein, Y. N.; Zhang, M.; Zakhidov, A. A.; Baughman, R. H. *Science* **2009**, *323*, 1575−1578.
(12) Zhang, H. X.; Feng, C.; Zhai, Y. C.; Jiang, K. L.; Li, Q. Q.; Fan, S. *Adv. Mater.* **2009**, *21*, 2299−2304.
(13) Ali, E. A.; Yuri, N. G.; Ray, H. B. *Nanotechnology* **2011**, *22*, 435704.
(14) Chen, L.; Liu, C.; Liu, K.; Meng, C.; Hu, C.; Wang, J.; Fan, S. *ACS Nano* **2011**, *5*, 1588−1593.

(15) Lehman, J. H.; Hurst, K. E.; Radojevic, A. M.; Dillon, A. C.; Osgood, J. R. M. *Opt. Lett.* **2007**, *32*, 772−774.
(16) Ragab, T.; Basaran, C. *J. Appl. Phys.* **2009**, *106*, 063705−063705.
(17) Jiang, J. W.; Wang, J. S. *J. Appl. Phys.* **2011**, *110*, 124319−124311.
(18) Knäbchen, A. *Phys. Rev. B* **1998**, *57*, 14630−14633.
(19) Bilotsky, Y.; Tomchuk, P. M. *Surf. Sci.* **2006**, *600*, 4702−4711.
(20) Bilotsky, Y.; Tomchuk, P. M. *Surf. Sci.* **2008**, *602*, 383−390.
(21) Arbouet, A.; Voisin, C.; Christofilos, D.; Langot, P.; Fatti, N. D.; Vallée, F.; Lermé, J.; Celep, G.; Cottancin, E.; Gaudry, M.; Pellarin, M.; Broyer, M.; Maillard, M.; Pileni, M. P.; Treguer, M. *Phys. Rev. Lett.* **2003**, *90*, 177401.
(22) Joung, S. K.; Okazaki, T.; Okada, S.; Iijima, S. *Phys. Status Solidi B* **2010**, *247*, 2700−2702.
(23) Lima, M. D.; Fang, S.; Lepró, X.; Lewis, C.; Ovalle Robles, R.; Carretero González, J.; Castillo Martínez, E.; Kozlov, M. E.; Oh, J.; Rawat, N.; Haines, C. S.; Haque, M. H.; Aare, V.; Stoughton, S.; Zakhidov, A. A.; Baughman, R. H. *Science* **2011**, *331*, 51−55.
(24) Ogoshi, T.; Ikeya, M.; Yamagishi, T. a.; Nakamoto, Y.; Harada, A. *J. Phys. Chem. C* **2008**, *112*, 13079−13083.
(25) Yang, L.; Xu, Y.; Wang, X.; Zhu, J.; Zhang, R.; He, P.; Fang, Y. *Anal. Chim. Acta* **2011**, *689*, 39−46.
(26) Hill, K. D. *Metrologia* **2002**, *39*, 51.
(27) Zhang, Z. B.; Li, J.; Cabezas, A. L.; Zhang, S. L. *Chem. Phys. Lett.* **2009**, *476*, 258−261.
(28) Yoon, Y. H.; Song, J. W.; Kim, D.; Kim, J.; Park, J. K.; Oh, S. K.; Han, C. S. *Adv. Mater.* **2007**, *19*, 4284−4287.
(29) Kim, D.; Lee, H. C.; Woo, J. Y.; Han, C. S. *J. Phys. Chem. C* **2010**, *114*, 5817−5821.
(30) Jang, H. S.; Jeon, S. K.; Nahm, S. H. *Carbon* **2011**, *49*, 111−116.
(31) Kang, T. J.; Kim, T.; Seo, S. M.; Park, Y. J.; Kim, Y. H. *Carbon* **2011**, *49*, 1087−1093.
(32) Sui, D.; Huang, Y.; Huang, L.; Liang, J.; Ma, Y.; Chen, Y. *Small* **2011**, *7*, 3186−3192.
(33) Zhang, Y.; Franklin, N. W.; Chen, R. J.; Dai, H. *Chem. Phys. Lett.* **2000**, *331*, 35−41.
(34) Aliev, A. E.; Guthy, C.; Zhang, M.; Fang, S.; Zakhidov, A. A.; Fischer, J. E.; Baughman, R. H. *Carbon* **2007**, *45*, 2880−2888.
(35) Korenblit, I. Y.; Gerber, A.; Milner, A.; Karpovsky, M. *Phys. Rev. B* **1999**, *59*, 131−134.
(36) Gerber, A.; Milner, A.; Korenblit, I. Y.; Karpovsky, M.; Gladkikh, A.; Sulpice, A. *Phys. Rev. B* **1998**, *57*, 13667−13673.